ACTIVE MEDIA

PACS numbers: 42.55.Lt; 42.60.Lh
DOI: 10.1070/QE2005v035n03ABEH002887

Optical characteristics of the gas-discharge plasma of working mixtures in an excimer HgBr/HgI radiation source

A.N. Malinin

Abstract. **The composition and partial pressures were determined for the components of gas mixtures which provide the maximum emission yield simultaneously at two wavelengths 502 nm and 444 nm in the self-heating regime of an excimer HgBr/HgI radiation source excited by a barrier discharge. The conditions for prolonged (no less than 4×10^6 pulses) stable operation at high pulse repetition rates $f = 0.5 - 10$ kHz are determined. Pulsed and average (for $f = 5$ kHz) output power densities of 270 W cm^{-3} and 65 mW cm^{-3}, respectively, and the pump-to-output power conversion efficiency of $\sim$30 % were achieved. The processes increasing the population of the upper $B^2\Sigma^+_{1/2}$ state of mercury monohalides are discussed.**

Keywords*: excimer laser, visible spectral range, working mixtures, gas-discharge plasma of a barrier discharge.*

1. Introduction

Despite the fact that excimer lasers have already existed for 30 years, high-power gas-discharge repetitively pulsed lasers emitting in the visible spectral region with a high pulse repetition rate have not been developed so far. Several practical applications, such as environment and water basin monitoring, ranging of objects in the sea, underwater communication, processing of electronics materials etc., require the development of high-power repetitively pulsed lasers emitting in the green – blue spectral region.

An excimer HgBr/HgI laser emitting simultaneously at 502 ± 20 nm and 444 ± 5 nm [1 – 4] may be a possible tool for the solution of the above problems. To design and develop high-power lasers, it is necessary to know the emission characteristics of the $HgBr^*$ and HgI^* molecules in the working mixtures of the active medium (gas-discharge plasma) at high pump pulse repetition rates. These molecules are excited in the gas-discharge plasma in collisions of plasma electrons with the molecules of mercury dihalides [5 – 9] in the reactions

$$\begin{aligned} &HgX_2 + e \rightarrow HgX^* + X + e, \\ &HgX_2 + e \rightarrow HgX^* + X^-, \end{aligned} \qquad (1)$$

where X is a halogen atom (Cl, Br, I).

A.N. Malinin Uzhgorod National University, ul. Pidgirna 46, 88000 Uzhgorod, Ukraine; e-mail: mal@univ.uzhgorod.ua

Received 20 September 2004
Kvantovaya Elektronika **35** (3) 243 – 251 (2005)
Translated by E.N. Ragozin

The energy and spectral characteristics of the gas-discharge plasma were found to change significantly upon addition of mercury dihalide vapour and gases to the working mixtures [1, 10 – 12]. These results stimulated complex investigations of the optical characteristics of the working mixtures of an excimer HgBr/HgI laser for optimising the energy characteristics of these mixtures in relation to the composition and partial pressures, the pump pulse repetition rate, and the energy deposition, which is presented in our paper.

2. Experimental

The emission characteristics of excimer $HgBr^*$ and HgI^* molecules in the working mixtures (mercury dihalide vapour, rare gases, and molecular nitrogen) of the HgBr/HgI radiation source were investigated in the gas-discharge plasma of a barrier discharge at the atmospheric pressure. Quartz glass was used as a barrier. Note that the barrier discharge was employed in high-power gas-discharge lasers based other mixtures [13]. In the mixtures under study, the barrier-discharge plasma was produced in the interelectrode space inside a 200-mm long quartz tube with a 2-mm thick wall and an external diameter of 34 mm (Fig. 1).

The separation between inner electrode (*4*) of round section (4 mm in diameter) and outer electrode (*2*) was 15 mm. The inner electrode was located on the tube axis and the outer electrode (perforated, with a radiation transmission coefficient of 72 %) on the tube surface. The tube ends were welded up; metal lead (*6*) supplying the

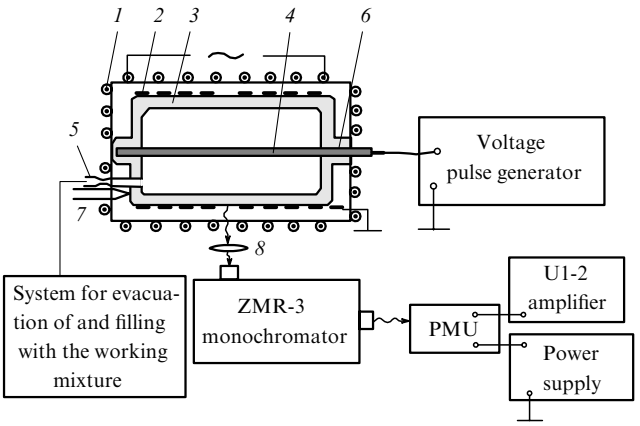

Figure 1. Scheme of the experimental setup: (*1*) electric heater; (*2*) outer (mesh) electrode; (*3*) cell; (*4*) inner electrode; (*5*) capillary; (*6*) metal lead; (*7*) thermocouple; (*8*) lens.

energy from a power source to the electrode, was welded in one of the ends. On the opposite end wall a quartz glass outlet with a 20-mm long capillary 1 mm in diameter was located, through which the tube was evacuated and filled (charged) with the mixture components under study.

The discharge was powered from a nanosecond pulse generator. A TG12-130/10 thyratron was employed as a switch. The storage capacitor was assembled of low-inductance KVI-3 capacitors. The capacitor was recharged via the primary winding of a step-up transformer with the 1 : 3 conversion coefficient. In the course of experiments, the pulsed voltage and current (with pulses ~ 150 ns in duration) across the cell electrodes were maintained approximately constant at 22 – 30 kV and 265 A, respectively, the pulse repetition rate was 0.5 – 5 kHz, and the capacitance of the storage capacitor was 1.36 nF.

The radiation was coupled out from the central region of the interelectrode space and analysed in the visible and near-UV spectral regions with a ZMR-3 monochromator equipped with a FEU-79 photomultiplier (Fig. 1). The amplitude – time radiation characteristics were studied by using a 14ELU-FS electron linear multiplier instead of a FEU-79 photomultiplier. The spectral resolution of the ZMR-3 monochromator was 44 Å at a wavelength of 434 nm. The optical system was calibrated using an SI8-200 tungsten reference band lamp with the filament temperature 2173 K.

The voltage and discharge current pulses of the radiation source were recorded with an S8-2 dual-beam oscilloscope, the signals to which were fed from a voltage divider and the integrating circuit of a calibrated Rogowski loop. The amplitude – time characteristics of the radiation in the 400 – 510 nm range separated with an SZS-8 optical filter were measured with an FEK-22SPU photocell. A diaphragm with an area of 1 cm^2 was placed in front of it. The average output power was measured with a Kvartz-01 power meter.

The power emitted from the entire surface of the radiation source was determined from the expression: $P_{rad} = \Omega_0 P_{rec} \Omega_{rec}^{-1}$, where P_{rec} is the power in watts measured with the photodetector; Ω_0 is the equivalent solid angle; $\Omega_{rec} = S_{rec}/l_0^2$ is the solid angle of the photodetector; S_{rec} is the area of the photodetector window; and l_0 is the distance between the radiation source and photodetector. The equivalent solid angle was taken to be π^2 (for a cylindrical surface) [14].

The mixtures under study were prepared directly in the interelectrode space by sequentially letting in a heavy xenon rare gas or nitrogen and a light helium buffer gas. Mercury dihalides (60 mg of the mercury dibromide $HgBr_2$ and 60 mg of the mercury diiodide HgI_2) were precharged into the interelectrode space. The surfaces of the elements of the internal tube volume were degassed by baking it at a temperature of 50 °C and evacuating to a residual gas pressure of 10^{-3} Torr for 2 h. The partial $HgBr_2$ and HgI_2 vapour pressure in the working mixtures was produced by mixture heating during the repetitively pulsed discharge energy dissipation, and in some experiments the mixture was heated with an electric heater (Fig. 1).The saturated vapour pressure of mercury dihalides was determined from the temperature of the coolest part of the tube by the linear interpolation of the reference data [15]. The partial gas pressures were measured with a standard membrane vacuum gauge or a manometer.

3. Experimental results and discussion

The characteristics of gas-discharge plasma emission were investigated for the multicomponent mixtures $HgI_2 - HgBr_2 - He$, $HgI_2 - HgBr_2 - Xe - He$, and $HgI_2 - HgBr_2 - N_2 - He$.

Figure 2 shows the plasma emission spectra of the barrier discharge in the mixture of mercury diiodide and dibromide vapours with helium for pump pulse repetition rates of 0.5, 2, and 4 kHz, and for the amplitudes of voltage across the electrodes and current through the gas discharge gap of 25.5 kV and 265 A, respectively. The total mixture pressure was 162 kPa.

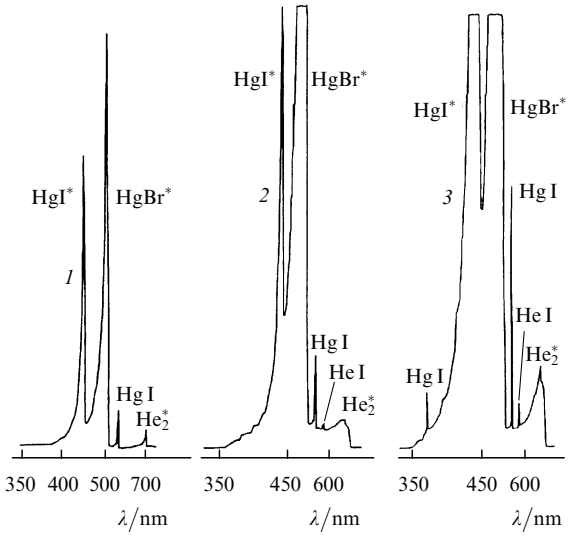

Figure 2. Plasma emission spectra of the barrier discharge in the $HgI_2 - HgBr_2 - He$ mixture for a pulse repetition rate of 500 (*1*), 2000 (*2*), and 4000 Hz (*3*), voltage and current amplitudes of 25.5 kV and 265 A, respectively, and the total mixture pressure of 162 kPa.

The emission spectra of this mixture exhibit the $B^2\Sigma^+_{1/2} \rightarrow X^2\Sigma^+_{1/2}$ vibronic bands of the $HgBr^*$ and HgI^* excimer molecules with maxima at 502 and 444 nm [16], the intensity of these bands abruptly increasing in the long-wavelength wing and slowly decreasing in the short-wavelength wing. The spectral bands cover the 370 – 510 nm wavelength range. When the pump pulse repetition rate was changed between 0.5 and 4 kHz, the shape, width, and positions of the spectral bands did not change; only their intensity and the ratio between the intensities at the edges of the bands were changed. In addition to these bands, the emission lines of atomic mercury at 365 and 546 nm (the $6p^3P^o_2 - 6d^3D_3$ and $7s^3S_1 - 6p^3P^o_2$ transitions [17, 18]), the 587-nm line of atomic helium (the $2p^3P_{2,1} - 3d^3D_{3,2,1}$ transition), and the emission bands of molecular helium (the upper transition levels are the quasibound or free states $A^1\Sigma^+_u$ [19]) in the long-wavelength region between 600 and 750 nm were observed. As the pump pulse repetition rate was increased from 500 to 4000 Hz, the intensity of the emission bands and lines increased.

Upon addition of molecular nitrogen (with a partial pressure of 1.52 kPa) and helium (160.4 kPa) to the mixture of mercury dibromide and diiodide, the emission intensity of mercury monohalide molecules was maximal for a pulse repetition rate of 2000 Hz. In this case, the emission

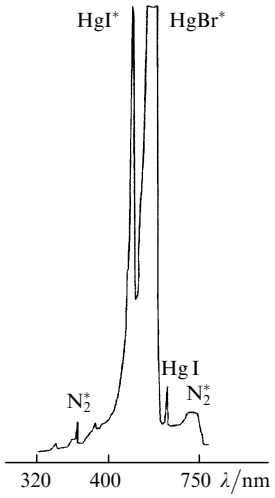

Figure 3. Emission spectrum of the $HgI_2 - HgBr_2 - N_2 - He$ mixture for partial pressures of mercury diiodide of 1.8 Pa, mercury dibromide of 7.6 Pa, nitrogen of 1.5 kPa, helium of 162 kPa, for a pulse repetition rate of 2000 Hz, and voltage and current amplitudes of 22 kV and 265 A, respectively.

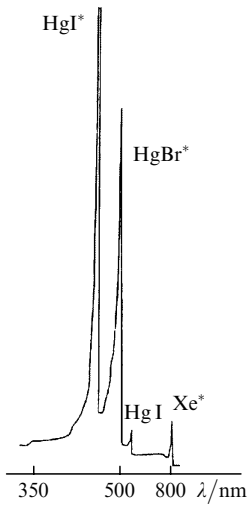

Figure 4. Emission spectrum of the $HgI_2 - HgBr_2 - Xe - He$ mixture for partial pressures of mercury diiodide of 7.5 Pa, mercury dibromide of 24.3 Pa, xenon of 7 kPa, helium of 162 kPa, for a pulse repetition rate of 2000 Hz, and voltage and current amplitudes of 22 kV and 265 A, respectively.

spectrum of the gas-discharge plasma (Fig. 3) exhibited the $B^2\Sigma^+_{1/2} \rightarrow X^2\Sigma^+_{1/2}$ vibronic bands of the $HgBr^*$ and HgI^* excimer molecules at 502 and 444 nm, the mercury line at 546 nm, and the emission bands of molecular nitrogen (N_2^*) at 337, 357, 375, and 654 nm, which correspond to the $C^3\Pi_u \rightarrow B^3\Pi_g$ transition (the second positive system) [16].

For the mixture with xenon $HgI_2 - HgBr_2 - Xe - He$ (the partial pressure of xenon was 1 kPa and of helium was 160.9 kPa), the plasma emission spectrum (Fig. 4) consisted of the systems of the $B^2\Sigma^+_{1/2} \rightarrow X^2\Sigma^+_{1/2}$ bands of the HgI^* and $HgBr^*$ molecules at 444 and 502 nm, respectively, and the lines of Hg atoms at 546 nm and Xe atoms at 823 nm (the $6s[3/2]^o_2 - 6p[3/2]_2$ transition) [16–18]. In addition, this mixture exhibited an increase of the emission intensity of the system of bands at 444 nm compared to its intensity in the spectrum of the discharge in the working $HgI_2 - HgBr_2 - He$ mixture.

As the pump pulse repetition rate was increased up to 4000 Hz in these experiments, the intensity of the emission bands of molecular nitrogen and the lines of atomic mercury and xenon in the mixtures also increased.

The emission bands and lines of the barrier-discharge plasma in the mixture of mercury dibromide and diiodide vapour with helium, xenon, and molecular nitrogen for a pump pulse repetition rate of 2000 Hz, their relative intensities I/k_λ, taking into account the spectral sensitivity k_λ of the detection system and their excitation energies are presented in Table 1.

Figures 5 and 6 demonstrate the dependences of the intensity ratios of the strongest 502-nm and 444-nm emission bands of the barrier-discharge plasma in the working mixture on the partial pressures of mercury dihalides. In these experiments, the partial pressures were varied at a constant pulse repetition rate by changing the temperature of the coolest part of the tube with the help of an external electric heater and converting the temperatures to the partial saturated vapour pressures of mercury dihalides according to the reference date [15]. As the partial pressure of mercury dihalides is increased, the emission intensity of mercury monoiodide and monobromide molecules increases, reaches its maximum, and decreases (Figs 5 and 6). The partial vapour pressures of mercury dihalides at which the emission intensity of mercury monohalides is maximum are different. For the HgI^* and $HgBr^*$ molecules, the pressures are 0.1 and 0.3 kPa, respectively. The maximum emission intensity for mercury monoiodide molecules is higher by 10 %. For high partial pressures of mercury dihalides, the rate of decrease of the emission intensity becomes lower: beginning with a partial vapour pressure of mercury diiodide of 0.9 kPa for the HgI^* molecules and beginning with a high partial vapour pressure of mercury dibromide (2.5 kPa) for the $HgBr^*$ molecules.

Table 1. Spectral bands and emission lines of the working mixtures of the HgBr/HgI radiation source.

λ/nm	Molecule, atom	k_λ (arb. units)	I/k_λ (arb. units)			E_{ex}/eV	References
			$HgI_2 - HgBr_2 - He$	$HgI_2 - HgBr_2 - Xe - He$	$HgI_2 - HgBr_2 - N_2 - He$		
337	N_2	1.7	–	–	0.07	11.05	[16]
357	N_2	1.9	–	–	0.34	11.05	[16]
375	N_2	2.6	–	–	0.23	11.05	[16]
444	Hg I	6	15	15.9	0.6	7.00	[6]
502	HgBr	16	6	4.6	1.8	6.00	[6]
546	Hg I	32.5	0.15	0.17	0.04	7.73	[17, 18]
654	N_2	67.5	–	–	0.001	9.14	[16]
823	Xe I	21	–	0.35	–	9.82	[17, 18]

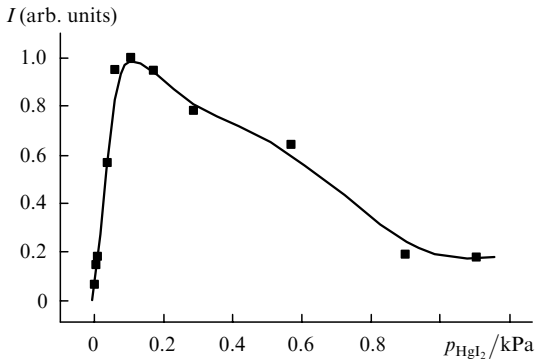

Figure 5. Emission intensity I of mercury monoiodide molecules as a function of the partial pressure p_{HgI_2} of mercury diiodide for the $HgI_2 - HgBr_2 - He$ mixture, voltage and current amplitudes of 25.5 kV and 265 A, respectively, a pump pulse repetition rate of 500 Hz, and a total mixture pressure of 162 kPa.

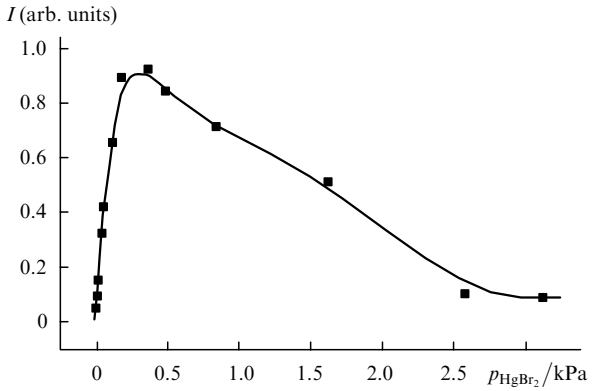

Figure 6. Emission intensity I of mercury monobromide molecules as a function of the partial pressure of mercury dibromide p_{HgBr_2} for the $HgI_2 - HgBr_2 - He$ mixture, voltage and current amplitudes of 25.5 kV and 265 A, respectively, a pump pulse repetition rate of 500 Hz, and a total mixture pressure of 162 kPa.

Figure 7 shows the emission intensities for the excimer molecules of mercury monoiodide and monobromide for the working mixture of the HgBr/HgI radiation source as functions of partial pressures of xenon and molecular nitrogen. The limits of variation of the partial pressures of gaseous mixture components were determined by the stability of a homogeneous discharge. The emission of these molecules is most intense when the partial xenon pressure is in the range of 1 kPa. For mixtures with molecular nitrogen, the emission intensity of the HgI^* and $HgBr^*$ molecules depends only slightly on the partial pressure of N_2 molecules. In mixtures with xenon, the emission of the mercury monoiodide molecules is stronger in contrast to the mixtures with nitrogen, where the intensity of mercury monobromide emission is higher.

The dependences of the emission intensity of mercury monohalides on the number of pump pulses are presented in Fig. 8 for mixtures of different composition (the gas component ratios were optimised to obtain the maximal emission intensities of the HgI^* and $HgBr^*$ molecules). The emission intensity saturation as a function of the number of pump pulses in mixtures of these molecules with xenon occurs later [curves (*1*) and (*2*) in Fig. 8] than in mixtures with molecular nitrogen [curves (*4*) and (*6*)]. For a mixture

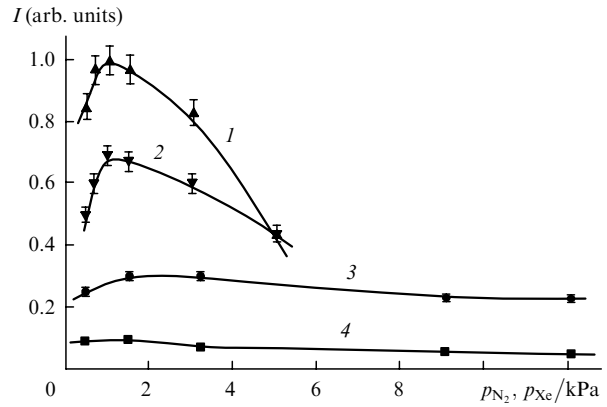

Figure 7. Emission intensities I of the molecules HgI^* (*1*, *3*) and $HgBr^*$ (*2*, *4*) as functions of the partial xenon pressure in the $HgI_2 - HgBr_2 - Xe - He$ mixture (*1*, *2*) and of the partial nitrogen pressure in the $HgI_2 - HgBr_2 - N_2 - He$ mixture (*4*, *3*) for a total mixture pressure of 162 kPa.

of the vapour of mercury dihalides only with helium, the emission intensity saturation for excimer molecules takes place even later [curves (*3*) and (*5*)]. In addition, the emission intensity of the excimer molecules HgI^* and $HgBr^*$ in mixtures with xenon is higher, the contribution of mercury monoiodide emission being dominant [curve (*1*)]. On the contrary, the contribution of mercury monobromide emission dominates in mixtures with nitrogen [curves (*4*) and (*6*), Table 1].

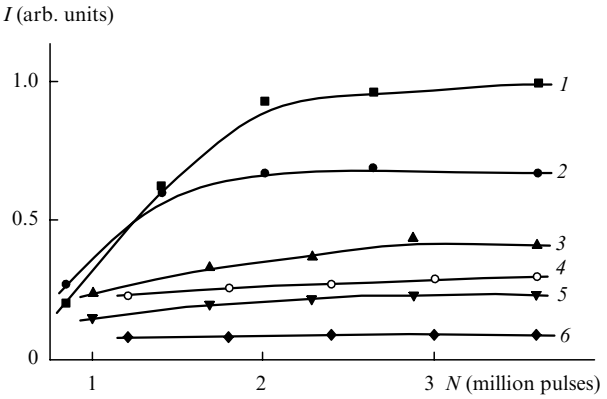

Figure 8. Dependence of the radiation intensity I on the total number N of pulses for mercury monohalides: for HgI^* molecules and the mixture $HgI_2 : HgBr_2 : Xe : He = 14.6$ Pa : 45.2 Pa : 1 kPa : 160.9 kPa (*1*), for $HgBr^*$ molecules and the mixture $HgI_2 : HgBr_2 : Xe : He =$ 14.6 Pa : 45.2 Pa : 1 kPa : 160.9 kPa (*2*), for HgI^* molecules and the mixture $HgI_2 : HgBr_2 : He = 12.9$ Pa : 39.8 Pa : 161.9 kPa (*3*), for $HgBr^*$ molecules and the mixture $HgI_2 : HgBr_2 : N_2 : He =$ 6.3 Pa : 21 Pa : 1.52 kPa : 160.4 kPa (*4*), for $HgBr^*$ molecules and the mixture $HgI_2 : HgBr_2 : He = 12.9$ Pa : 39.8 Pa : 161.9 kPa (*5*), and for HgI^* molecules and the mixture $HgI_2 : HgBr_2 : N_2 : He =$ 6.3 Pa : 21 Pa : 1.52 kPa : 160.4 kPa (*6*). The total mixture pressure was 162 kPa and the pump pulse repetition rate was 2000 Hz.

To elucidate the effect of composition and partial pressures of the mixture components on the shape and duration of the radiation pulse of the working mixtures of the HgBr/HgI laser, we investigated the amplitude–time radiation characteristics of the excimer molecules HgI^* and $HgBr^*$ separately. The results of these investigations are

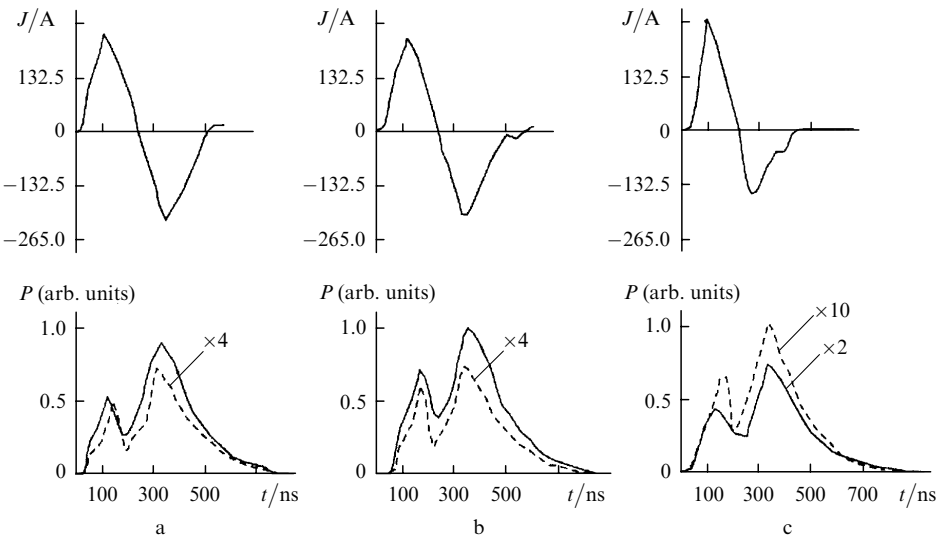

Figure 9. Oscilloscope traces of the current J and output power P pulses for HgI^* (dashed curves) and $HgBr^*$ (solid curves) molecules for the mixtures $HgI_2 : HgBr_2 : He = 13.1$ Pa : 45.2 Pa : 142 kPa (a), $HgI_2 : HgBr_2 : Xe : He = 13.1$ Pa : 45.3 Pa : 3.04 kPa : 159.9 kPa (b), and $HgI_2 : HgBr_2 : N_2 : He =$ 5.5 Pa : 23.4 Pa : 9.1 kPa : 152.9 kPa (c).

given in Fig. 9 and Table 2. The error and reproducibility of the results of oscillographic measurements were 10 % and 90 %, respectively. For each mixture, the pulses of discharge current were bipolar in shape and had an amplitude of 265 A and a duration of 150 ns.

The emission intensity of the HgI^* and $HgBr^*$ excimer molecules exhibited a double-humped time dependence. The maxima of the emission power and the absolute value of current coincide in time. For these molecules, the second radiation pulse amplitude is higher than the first one both in mixtures of mercury dihalides with helium and in their mixtures with additions of xenon and molecular nitrogen (Fig. 9, Table 2). All the mixtures were characterised by an increase of duration ($\Delta\tau$) of the second radiation pulse compared to the duration of the first one. In the mixture of mercury dihalides with xenon and helium, the first-to-second pulse amplitude ratio for the HgI^* molecules is different. The difference between the amplitudes of these pulses becomes smaller; furthermore, the duration of the trailing edge τ increases. In the mixture of mercury dihalides with nitrogen and helium, the observed amplitudes of both pulses become lower (in this case, the second pulse is stronger than the first one) and the trailing edge of the second pulse becomes longer. The amplitude – time characteristics of the emission of the excimer molecule $HgBr^*$ is characterised by the same, as for the excimer molecule HgI^*, dependence of the pulse amplitudes and lengths on the mixture composition, with the exception of the mixture with addition of xenon (the first-to-second pulse amplitude ratio does not change).

The average emission power in the 400 – 510 nm spectral range, separated with an SZS-8 optical filter, as a function of helium pressure is shown in Fig. 10 for the $HgI_2 - HgBr_2 - He$ mixture. As the partial helium pressure was increased from 140 to 200 kPa, the average power increased, achieved maximum at 180 kPa, and then decreased. As the voltage across the electrodes and pump pulse repetition rate were increased, the average radiation power increased (Figs 11 and 12). For a voltage of 30 kV it amounts to 11 W for a pulse repetition rate of 2 kHz and to 22.5 W for a pulse repetition rate of 5 kHz. The radiation power in a single pulse amounts to 93 kW (with a specific power of 270 W cm^{-3}) for a total mixture pressure of 162 kPa, current and voltage amplitudes of 265 A and 22.5 kV, respectively, and a pulse repetition rate of 2 kHz. The power deposited into the working medium is converted to radiation with an efficiency of 30 %.

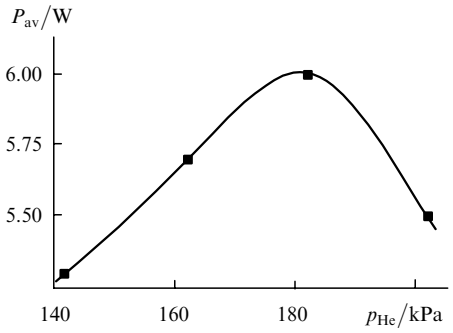

Figure 10. Average output radiation power P_{av} as a function of partial pressure p_{He} of helium for a pump pulse repetition rate of 2000 Hz and a voltage amplitude of 22.5 kV.

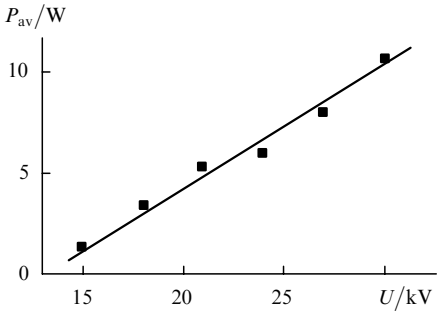

Figure 11. Average output radiation power P_{av} as a function of voltage amplitude U for a pulse repetition rate of 2000 Hz and a total mixture pressure of 162 kPa.

Table 2. Amplitude–time radiation characteristics of the HgI^* and $HgBr^*$ excimer molecules in the working mixtures of the HgBr/HgI radiation source for a pump pulse repetition rate of 2 kHz.

Mixture	Partial pressure of the gaseous components/kPa	Source temperature/°C	Molecule	Partial pressures of halides/Pa	τ/ns	$\Delta\tau$/ns	Amplitudes of the two pulses (arb. units)
$HgI_2 - HgBr_2 - He$	122	116.5	HgI	10.8	238	150	1.3
						163	1.7
			HgBr	37.4	225	163	3.8
						213	5.5
	142	119	HgI	13.1	325	100	1
						186	1.4
			HgBr	45.2	325	150	3.9
						212	5.6
	162	117	HgI	12.1	425	88	2.4
						181	3.3
			HgBr	37.4	225	193	4
						175	6.5
	182	120	HgI	14.6	238	75	0.81
						200	0.95
			HgBr	45.3	188	100	3.3
						150	4.6
$HgI_2 - HgBr_2 - N_2 - He$ (total pressure of 162 kPa)	0.5	119.5	HgI	13.1	300	94	0.48
						200	0.75
			HgBr	45.3	300	164	1.58
						188	2.75
	1.52	118.5	HgI	12.2	388	94	0.35
						213	0.56
			HgBr	40.7	413	88	1.16
						275	2.5
	3.24	116.5	HgI	10.8	413	88	0.33
						175	0.55
			HgBr	33.6	500	88	1.1
						250	2.7
	9.1	109	HgI	5.5	513	88	0.21
						375	0.41
			HgBr	23.4	563	88	1.1
						312	2.83
$HgI_2 - HgBr_2 - Xe - He$ (total pressure of 162 kPa)	0.5	129.5	HgI	28.3	288	81	0.95
						238	1.16
			HgBr	87.5	250	164	3.9
						188	5.16
	1.01	121.5	HgI	14.6	288	138	0.98
						175	1
			HgBr	54.8	263	63	3.6
						200	5
	3.04	120	HgI	13.1	275	63	1.13
						213	1.16
			HgBr	45.3	288	113	4.3
						225	5.6
	5.06	124	HgI	17.3	288	75	0.64
						150	0.66
			HgBr	65	275	100	2.41
						194	3.16

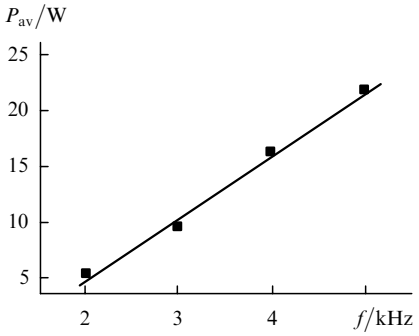

Figure 12. Average output radiation power P_{av} as a function of the pulse repetition rate f for a total mixture pressure of 162 kPa and a voltage amplitude of 22.5 kV.

The changes in the emission band intensities of the $HgBr^*$ and HgI^* excimer molecules and in the average radiation power of the gas-discharge plasma of the active medium of the HgBr/HgI radiation source with pump pulse repetition rate (Figs 2 and 12) are caused by the increase in the number of electron-excitation events of the molecular and atomic plasma components and accordingly in the number of output radiation photons recorded per unit time. In addition, these changes occur due to the change in the active medium temperature (the discharge-energy dissipation power increases with pump pulse repetition rate [20] and the partial pressures of mercury dihalides are accordingly increase [15]). The partial component pressure ratios also change: for the HgI_2: $HgBr_2$: He mixture at pulse repetition rates of 500, 2000, and 4000 Hz, they are 0.6 Pa : 2.7 Pa : 162 kPa, 6.8 Pa : 23.4 Pa : 162 kPa, and 14.6 Pa : 49.2 Pa : 162 kPa, respectively. This in turn results in the increase in mercury dihalide vapour densities and eventually leads to different densities of the excited HgI^* and $HgBr^*$ molecules in the $B^2\Sigma^+_{1/2}$ state, which changes the emission band intensities and the average radiation power in the 400–510 nm spectral range (Fig. 12).

The presence of the 546-nm line of atomic Hg in the emission spectra (Figs 2–4) may be caused by the degradation of working mixtures. The molecules of mercury monoiodide and monobromide do not have time to associate in the processes

$$HgX(X^2\Sigma^+_{1/2}) + X_2 \rightarrow HgX_2 + X, \quad (2)$$

$$HgX(X^2\Sigma^+_{1/2}) + X + R \rightarrow HgX_2 + R \quad (3)$$

(where X = I, Br, R is the helium buffer gas) and dissociate into mercury and halogen atoms in collisions with electrons in the gas-discharge plasma [21]. The halogen atoms have time to travel to the electrode of the radiation source and form metal halides [22]. Mercury atoms are accumulated and excited in electron collisions to emit at 546 nm.

The dependences of the emission intensity of the HgI^* and $HgBr^*$ molecules on the partial pressures of mercury diiodide (Fig. 5) and dibromide (Fig. 6) and the optimal partial pressures of mercury diiodide and dibromide are determined by the kinetics of the processes responsible for the excitation and quenching of the $B^2\Sigma^+_{1/2}$ state of these molecules and by the rate constants of excitation and quenching

$$HgX^* + M \rightarrow HgX + M + \Delta E, \quad (4)$$

where M is the amount of quenching molecules (mercury diiodide and dibromide); ΔE is the energy difference in the reaction.

When the partial pressures of mercury dihalides exceed a certain value, the quenching process (4) plays an important role, resulting in the decrease in the emission intensity. The different partial pressures of mercury dihalides at which the maximum emission intensity of mercury monohalides is achieved are determined by the quenching rate constants, which are unknown for multicomponent mixtures. The decrease in the rate of emission intensity lowering at high partial pressures (Figs 5 and 6) of mercury dihalides (0.9 kPa for HgI^* molecules and 2.5 kPa for $HgBr^*$ molecules) cannot be explained by the experimental data. This question can be elucidated with the help of numerical calculations of specific losses of discharge power in different channels as a function of plasma component densities, which will be the subject of further investigations.

The emission intensity of the HgI^* molecules is higher than that of the $HgBr^*$ molecules (Table 1, Figs 7 and 8, the $HgI_2 - HgBr_2 - He$ and $HgI_2 - HgBr_2 - Xe - He$ mixtures). At the same time, the ratio between the electron excitation rate constants for the $B^2\Sigma^+_{1/2}$ states of these molecules in the binary $HgBr_2 - He$ and $HgI_2 - He$ mixtures is different (for the HgI^* molecule, the rate constant is approximately one order of magnitude lower [9]). This may be attributed to the existence of an additional excitation mechanism [apart from the main mechanism (1)] for the HgI^* molecules. This additional mechanism may involve population transfer from the $HgBr^*$ molecules at higher levels [10, 23] in collisions with mercury diiodide molecules (the energy difference between the $B^2\Sigma^+_{1/2}$ states of mercury monobromide and mercury monoiodide is equal to ~ 0.2 eV):

$$HgBr^* + HgI_2 \rightarrow HgI_2^* \rightarrow HgI^* + I + HgBr$$

$$\rightarrow HgI + I + HgBr + h\nu + \Delta E, \quad (5)$$

where ΔE is the energy difference of the $HgBr^*$ and HgI^* molecules in the $B^2\Sigma^+_{1/2}$ states.

In the mixtures of mercury diiodide and dibromide with xenon and helium, the emission intensity of HgI^* molecules is even higher (Figs 7 and 8, Table 1). This is caused by the quenching of the $C^2\Pi^+_{1/2}$ state of mercury monoiodide by xenon with population transfer to the $B^2\Sigma^+_{1/2}$ state:

$$HgI(C^2\Pi^+_{1/2}) + Xe \rightarrow HgI(B^2\Sigma^+_{1/2}) + Xe + \Delta E, \quad (6)$$

where ΔE is the excitation energy difference of the $C^2\Pi^+_{1/2}$ and $B^2\Sigma^+_{1/2}$ states of the HgI^* molecule. This process was observed in experiments on mercury diiodide photodissociation [24, 25]. The quenching process (6) contributes, in addition to the main process (1), to the state populations of the HgI^* molecules.

In mixtures of mercury dihalides with helium and xenon, the emission intensity of the $HgBr^*$ molecules is higher than in mixtures without xenon {Figs 7 and 8 [curves (*2*)], Table 1}. This may be attributed to the existence of an additional excitation mechanism [apart from the main mechanism (1)] for the $HgBr^*$ molecules in these mixtures,

namely, to the population transfer from the metastable $^3P_2$ state of atomic xenon in the reaction [26]

$$Xe^* + HgBr_2 \rightarrow HgBr_2^* + Xe \rightarrow HgBr^* + Br + Xe$$

$$\rightarrow HgBr + Br + h\nu + Xe. \quad (7)$$

The higher emission intensity of the excimer $HgBr^*$ molecules compared to the HgI^* molecules in the $HgBr_2-HgI_2-N_2-He$ mixture is due to the fact that the rate constant for the population transfer from the nitrogen molecule in the metastable state N_2 ($A^3\Sigma_u^+$) in the reaction [26]

$$N_2^* + HgBr_2 \rightarrow HgBr_2^* + N_2 \rightarrow HgBr^* + Br + N_2$$

$$\rightarrow HgBr + Br + h\nu + N_2 \quad (8)$$

is greater than the rate constant in the reaction

$$N_2^* + HgI_2 \rightarrow HgI_2^* + N_2 \rightarrow HgI^* + I + N_2$$

$$\rightarrow HgI + I + h\nu + N_2. \quad (9)$$

The dependence of emission intensity of the HgI^* and $HgBr^*$ molecules on the partial pressures of xenon and molecular nitrogen (Fig. 7) is determined by the efficiency of several processes responsible for the excitation and quenching of the $B^2\Sigma_{1/2}^+$ states of these molecules in the gas-discharge plasma of a barrier discharge [20]. The sharper decrease of the emission intensity with increasing the partial xenon pressure compared to the pressure of molecular nitrogen may be due to a higher rate constant for quenching of the HgI^* and $HgBr^*$ molecules by xenon atoms than by molecular nitrogen. The rate constants for the quenching of the HgI^* and $HgBr^*$ molecules by xenon are 2.2×10^{-13} and 3.8×10^{-14} cm^3 s^{-1} and by nitrogen are 2.9×10^{-14} and less than 3.4×10^{-14} cm^3 s^{-1}, respectively [24].

An earlier saturation of the emission intensity of HgI^* and $HgBr^*$ molecules with the number of pulses for mixtures with molecular nitrogen and xenon [Fig. 8, curves (*1*), (*2*), (*4*), (*6*)] than for three-component mixtures [curves (*3*), (*5*)] is due to different discharge energy dissipation rates for multicomponent plasmas. This rate depends primarily on the probabilities of elastic electron collisions with plasma components [9, 20]. The probabilities for these electron collisions with xenon atoms and nitrogen molecules are higher, which explains, to a first approximation, the dependences obtained. To determine the quantitative characteristics of these relations requires conducting numerical kinetic calculations of discharge energy dissipation in multicomponent mixtures.

The time dependence of current pulses (Fig. 9) is determined by the recharging of the dielectric–plasma circuit. The higher amplitudes of the second radiation pulse in comparison with the first one (Fig. 9, Table 2), its duration, and the length of its trailing edge are related to the increase in $B^2\Sigma_{1/2}^+$-state population of the molecules HgI^* and $HgBr^*$,which takes place after the main process (the dissociative excitation of these molecules by electrons in collisions with the molecules of mercury dihalides):

$$HgX_2^+ + e \rightarrow HgX(B^2\Sigma_{1/2}^+) + X, \quad (10)$$

$$HgX_2^+ + X^- \rightarrow HgX(B^2\Sigma_{1/2}^+) + X_2, \quad (11)$$

$$HgX(X^2\Sigma_{1/2}^+) + e \rightarrow HgX(B^2\Sigma_{1/2}^+) + e. \quad (12)$$

The authors of paper [1] believe that the recombination of positive ions of mercury dihalides with electrons (10) can play a significant role at current densities of ~ 1000 A cm^{-2}, which is not observed under our experimental conditions. The calculated rate constant for positive–negative ion recombination (11) is high (for the $HgBr_2$ molecule it is equal to $\sim 3 \times 10^{-7}$ cm^3 s^{-1}). However, this process plays a minor role in the conditions of a gas discharge because of the low atomic ion densities (the rate constant for negative Br^- ion production is equal to $\sim 10^{-10}$ cm^3 s^{-1} [5]). The electron excitation of the radicals $HgX(X^2\Sigma_{1/2}^+)$ to the $B^2\Sigma_{1/2}^+$ state (12) is possible under our experimental conditions. The radical density during the action of a current pulse (during the action of electrons) is determined by the rates of dissociative decomposition of mercury dihalides to the $X^2\Sigma_{1/2}^+$ state of mercury monohalides, radiation in the $B \rightarrow X$ transition, recovery of mercury dihalides, and quenching of the $B^2\Sigma_{1/2}^+$ state of mercury monohalides, respectively:

$$HgX_2 + e \rightarrow HgX(X^2\Sigma_{1/2}^+) + X + e, \quad (13)$$

$$HgX(B^2\Sigma_{1/2}^+) \rightarrow HgX(X^2\Sigma_{1/2}^+) + h\nu, \quad (14)$$

$$HgX(X^2\Sigma_{1/2}^+) + X + M \rightarrow HgX_2 + M, \quad (15)$$

$$HgX(X^2\Sigma_{1/2}^+) + X_2 + M \rightarrow HgX_2 + X + M, \quad (16)$$

$$HgX(B^2\Sigma_{1/2}^+) + M \rightarrow HgX(X^2\Sigma_{1/2}^+) + M + \Delta E, \quad (17)$$

where M is an atom or a molecule (He, HgI_2, $HgBr_2$) [9, 21, 27].

In the three-component mixture, the temporal broadening of the second pulse and its trailing edge is caused by the lowering of association rate of the diatomic molecules of mercury monohalides in the reactions (2), (3) and accordingly the accumulation of mercury monohalides in the ground state. This eventually results in the change of the temporal behaviour of the second pulse because of the increase in the $B^2\Sigma_{1/2}^+$-state population of mercury monohalides due to electron excitation from the $X^2\Sigma_{1/2}^+$ state.

The existence of optimal partial pressure for the helium buffer gas (Fig. 10) is related to the dynamics of discharge energy that is spent for heating the mixture of the vapour of two mercury dihalides and helium and to the quenching dynamics of the $B^2\Sigma_{1/2}^+$-state of mercury monohalides [20]. The increase in the average power with pump pulse voltage amplitude (Fig. 11) is caused by the increase in discharge power deposited into the dissociative excitation of mercury monohalides with increasing the parameter E/p [9].

4. Conclusions

The comprehensive study of the optical characteristics of the working mixtures of the HgBr/HgI radiation source has given the component composition and the quantitative

relations between partial component pressures in the mixture that maximise the radiation output at 502 and 444 nm. This mixture is the mercury diiodide and dibromide vapour mixture with helium and xenon $HgI_2 : HgBr_2 : Xe : He = 14.6\,Pa : 45.2\,Pa : 1\,kPa : 160.9\,kPa$.

A specific radiation power of 270 W cm^{-3} in one pulse and an average power of 65 mW cm^{-3} were achieved for a pump pulse repetition rate of 5 kHz; the pump-to-radiation power conversion efficiency is equal to $\sim 30\,\%$. The self-heating regime of the working mixtures of the HgBr/HgI excimer radiation source was realised for the first time. The conditions were found for a long-term (no less than 106 pulses) stable operation of the mixtures under investigation for high (0.5 – 10 kHz) pump pulse repetition rates. Additional processes are discussed which increase the population of the upper $B^2\Sigma^+_{1/2}$ state of mercury monohalides in the gas-discharge plasma of the working HgBr/HgI radiator mixtures, specifically: the excitation mercury monoiodide molecules (the $B^2\Sigma^+_{1/2}$ state); the population transfer from the $B^2\Sigma^+_{1/2}$ state of molecular mercury monobromide and the quenching of the $C^2\Pi_{1/2}$ state by xenon with population transfer to its $B^2\Sigma^+_{1/2}$ state as well as the excitation of the $B^2\Sigma^+_{1/2}$ state of mercury monobromide molecules due to population transfer from the metastable $^3P_2$ state of atomic xenon.

Acknowledgements. The author thanks A.V. Polyak for his assistance in the preparation of the paper.

References

1. Burnham R., Schimitschek E.J. *Laser Focus*, (6), 54 (1981).
2. Berry A.J., Whitehurst C., King T.A. *J. Phys. D: Appl. Phys.*, **21**, 39 (1988).
3. Petrukhin A.E., Podsosonnyi A.S. *Kvantovaya Elektron.*, **17**, 535 (1990) [*Sov. J. Quantum Electron.*, **20**, 467 (1990)].
4. Bazhulin S.P., Basov N.G., Bugrimov S.N., Zuev V.S., Kamrukov A.S., Kashnikov G.N., Kozlov N.P., Ovchinnikov P.A., et al. *Kvantovaya Elektron.*, **13**, 1515 (1986) [*Sov. J. Quantum Electron.*, **16**, 990 (1986)].
5. Malinin A.N., Shimon L.L. *Kvantovaya Elektron.*, **23**, 1077 (1996) [*Quantum Electron.*, **26**, 1047 (1996)].
6. Malinin A.N. *Laser Phys.*, **7**, 1032 (1997).
7. Malinin A.N., Shuaibov A.K., Shevera V.S. *Kvantovaya Elektron.*, **10**, 1495 (1983) [*Sov. J. Quantum Electron.*, **13**, 877 (1983)].
8. Kushawaha V., Mahmmood M. *J. Appl. Phys.*, **57**, 2173 (1987).
9. Malinin A.N. *Laser Phys.*, **8**, 395 (1998).
10. Malinin A.N., Guivan N.N., Shimon L.L. *Opt. Spektrosk.*, **89**, 905 (2000).
11. Malinin A.N., Guivan N.N., Shimon L.L., Polyak A.V., Zubrilin N.G., Shchedrin A.I. *Opt. Spektrosk.*, **91**, 922 (2001).
12. Malinin A.N., Polyak A.V., Guivan N.N., Zubrilin N.G., Shimon L.L. *Kvantovaya Elektron.*, **32**, 155 (2002) [*Quantum Electron.*, **32**, 155 (2002)].
13. Takenaka Y., Kuzumoto M., Yusui K., Yagi S., Tagashira M. *IEEE J. Quantum Electron.*, **27**, 2482 (1991).
14. Sapozhnikov R.A. *Teoreticheskaya fotometriya* (Theoretical Photometry) (Moscow: Energiya, 1977) p. 264.
15. Efimov A.I., Belorukova L.P., Vasil'kova I.V., Chechev V.P. *Svoistva neorganicheskikh soedinenii. Spravochnik*. (Handbook on Properties of Inorganic Compounds) (Leningrad: Khimiya, 1983) p. 392.
16. Pears R.W., Gaydon A.G. *The Identification of Molecular Spectra* (London: Chopman Hall LTD, 1963) p. 347.
17. Zaidel' A.N., Prokof'ev V.K., Raiskii S.M., Slavnyi V.A., Shreider E.Ya. *Tablitsy spektral'nykh linii* (Tables of Spectral Lines) (Moscow: Nauka, 1977) p. 800.
18. Prokop'ev V.E., Yatsenko A.S. Preprint (161) (Novosibirsk, IAE SO AN SSSR, 1981) p. 52.
19. Rhodes C.K. (Ed.) *Excimer Lasers* (New York: Springer-Verlag, 1979).
20. Raizer Yu.P. *Gas Discharge Physics* (Berlin: Springer-Verlag, 1991; Moscow: Nauka, 1987) p. 592.
21. Erlason A.C., Cool T.A. *Chem. Phys. Lett.*, **96**, 685 (1983).
22. Liu C.S., Liberman I. *Quantum Electron.*, **23**, 245 (1987).
23. Polyak A.V., Guivan M.M., Malinin O.M. *Nauk. Visnik Uzhgorod. Univ. Ser. Fiz.*, **7**, 131 (2000).
24. Roxlo C., Mandl A. *J. Chem. Phys.*, **72**, 541 (1980).
25. Bazhulin S.P., Basov N.G., Bugrimov S.N., Zuev V.S., Kamrukov A.S., Kashnikov G.N., Kozlov N.P., Ovchinnikov P.A., Opekan A.G., Orlov V.L., Protasov Yu.S. *Kvantovaya Elektron.*, **13**, 1017 (1986) [*Sov. J. Quantum Electron.*, **16**, 663 (1986)].
26. Chang R.S.T., Burnham R. *Appl. Phys. Lett.*, **36**, 397 (1980).
27. Malinin A.N. *Laser Phys.*, **7**, 1177 (1997).